Integration of polymer microlens array at fiber bundle extremity by photopolymerization

Xinhua Zeng,[1,2*] Jérôme Plain,[1,4] Safi Jradi,[1] Claire Darraud[3], Fréderic Louradour[3], Renaud Bachelot,[1] and Pascal Royer[1]

[1] *Laboratoire de Nanotechnologie et d'Instrumentation Optique, ICD, Université de Technologie de Troyes, 12, Rue Marie Curie, 10000 Troyes France*
[2] *Institute of Intelligent Machines, Chinese Academy of Sciences, Hefei, Anhui 230031, China*
[3] *Université de Limoges, CNRS, XLIM Institut de Recherche, 123 Ave. A. Thomas, F-87060 Limoges, France*
[4] *jerome.plain@utt.fr*
**xhzeng@iim.ac.cn or*

Abstract: We present a novel route to directly integrate an array of microlenses at the extremity of an optical fiber bundle. The method is based on photopolymerization at the end of the fiber. The method is based on the control of exposure dose and volume of the deposited droplet of photopolymerizable formulation. Optical properties of the integrated microlenses are discussed on the basis of FDTD calculations.

OCIS codes: (160.5470) Polymers; (060.2340) Fiber optics components; (040.1240) Arrays; (060.2350) Fiber optics imaging.

References and links

1. G. Lippmann, "Epreuves reversibles donnant la sensation du relief," J. Phys. Theor. Appl. **7**(1), 821–825 (1908).
2. J. W. Goodman, A. R. Dias, and L. M. Woody, "Fully parallel, high-speed incoherent optical method for performing discrete Fourier transforms," Opt. Lett. **2**(1), 1–3 (1978).
3. J. D. Rees, "Non-Gaussian imaging properties of GRIN fiber lens arrays," Appl. Opt. **21**(6), 1009–1012 (1982).
4. Y. Ishihara, and K. Tanigaki, "A high sensitivity IL-CCD image sensor with monolithic resin lens array", In Proceedings of IEEE IEDM. Tech. Dig. 497–500 (1983).
5. D. Daly, R. F. Stevens, M. C. Hutley, and N. Davues, "The manufacture of microlenses by melting photoresist," Meas. Sci. Technol. **1**(8), 759–766 (1990).
6. M. He, X. C. Yuan, N. Q. Ngo, J. Bu, and S. H. Tao, "Low-cost and efficient coupling technique using reflowed sol-gel microlens," Opt. Express **11**(14), 1621–1627 (2003).
7. H. Y. Lin, Y. H. Ho, J. H. Lee, K. Y. Chen, J. H. Fang, S. C. Hsu, M. K. Wei, H. Y. Lin, J. H. Tsai, and T. C. Wu, "Patterned microlens array for efficiency improvement of small-pixelated organic light-emitting devices," Opt. Express **16**(15), 11044–11051 (2008).
8. J. Arai, H. Kawai, and F. Okano, "Microlens arrays for integral imaging system," Appl. Opt. **45**(36), 9066–9078 (2006).
9. A. D. Ducharme, "Microlens diffusers for efficient laser speckle generation," Opt. Express **15**(22), 14573–14579 (2007).
10. J. W. Pan, C. M. Wang, H. C. Lan, W. S. Sun, and J. Y. Chang, "Homogenized LED-illumination using microlens arrays for a pocket-sized projector," Opt. Express **15**(17), 10483–10491 (2007).
11. D. Radtke, J. Duparré, U. D. Zeitner, and A. Tünnermann, "Laser lithographic fabrication and characterization of a spherical artificial compound eye," Opt. Express **15**(6), 3067–3077 (2007).
12. M. J. Aernecke, and D. R. Walt, "Optical-fiber arrays for vapor sensing," Sens. Actuators B **142**(2), 464–469 (2009).
13. V. Guieu, F. Lagugné-Labarthet, L. Servant, D. Talaga, and N. Sojic, "Ultrasharp optical-fiber nanoprobe array for Raman local-enhancement imaging," Small **4**(1), 96–99 (2008).
14. A. Chovin, P. Garrigue, P. Vinatier, and N. Sojic, "Development of an ordered array of optoelectrochemical individually readable sensors with submicrometer dimensions: application to remote electrochemiluminescence imaging," Anal. Chem. **76**(2), 357–364 (2004).
15. C. Amatore, A. Chovin, P. Garrigue, L. Servant, N. Sojic, S. Szunerits, and L. Thouin, "Remote fluorescence imaging of dynamic concentration profiles with micrometer resolution using a coherent optical fiber bundle," Anal. Chem. **76**(24), 7202–7210 (2004).
16. E. P. Chan, and A. J. Crosby, "Fabricating microlens arrays by surface wrinkling," Adv. Mater. **18**(24), 3238–3242 (2006).
17. O. J. Cayre, and V. N. Paunov, "Fabrication of microlens arrays by gel trapping of self-assembled particle monolayers at the decane–water interface," J. Mater. Chem. **14**(22), 3300–3302 (2004).
18. W. R. Cox, T. Chen, and D. J. Hayes, "Micro-optics fabrication by ink-jet printing," Opt. Photonics News 32–35 (2001).

#136713 - $15.00 USD Received 20 Oct 2010; revised 14 Feb 2011; accepted 15 Feb 2011; published 28 Feb 2011

19. M. Yaegashi, M. Kinoshita, A. Shishido, and T. Ikeda, "Direct fabrication of microlens arrays with polarization selectivity," Adv. Mater. **19**(6), 801–804 (2007).
20. H. Ottevaere, B. Volckaerts, J. Lamprecht, J. Schwider, A. Hermanne, I. Veretennicoff, and H. Thienpont, "Two-dimensional plastic microlens arrays by deep lithography with protons: fabrication and characterization," J. Opt. A, Pure Appl. Opt. **4**(4), 354–28 (2002).
21. J. R. Epstein, and D. R. Walt, "Fluorescence-based fibre optic arrays: a universal platform for sensing," Chem. Soc. Rev. **32**(4), 203–214 (2003).
22. E. W. Adams, J. Ueberfeld, D. M. Ratner, B. R. O'Keefe, D. R. Walt, and P. H. Seeberger, "Encoded fiber optic microsphere arrays for probing protein-carbohydrate interactions," Angew. Chem. **115**(43), 5475–5478 (2003).
23. D. R. Walt, T. M. Blicharz, R. B. Hayman, D. M. Rissin, M. Bowden, W. L. Siqueira, E. J. Helmerhorst, N. Grand-Pierre, F. G. Oppenheim, J. S. Bhatia, F. F. Little, and J. S. Brody, "Microsensor arrays for saliva diagnostics," Ann. N. Y. Acad. Sci. **1098**(1), 389–400 (2007).
24. C. N. LaFratta, and D. R. Walt, "Very high density sensing arrays," Chem. Rev. **108**(2), 614–637 (2008).
25. D. R. Walt, "Fibre optic microarrays," Chem. Soc. Rev. **39**(1), 38–50 (2009).
26. R. Bachelot, C. Ecoffet, D. Deloeil, P. Royer, and D. J. Lougnot, "Integration of micrometer-sized polymer elements at the end of optical fibers by free-radical photopolymerization," Appl. Opt. **40**(32), 5860–5871 (2001).
27. X. H. Zeng, J. Plain, S. Jradi, P. Renaud-Goud, R. Deturche, P. Royer, and R. Bachelot, "High speed sub-micrometric microscopy using optical polymer microlens," Chin. Opt. Lett. **7**, 901–903 (2009).
28. D. Chandra, S. Yang, and P. C. Lin, "Strain responsive concave and convex microlens arrays," Appl. Phys. Lett. **91**(25), 251912-1-251912-3 (2007).

1. Introduction

The use of very small lenses array was first suggested by Lippmann [1] in 1908 as an approach for 'Integral Photography'. Since, the domain of microlens array (MLAs) has given rise to increasing interest, especially over the past 40 years. For example, they are of first importance in digital optical processing and optical computing (Goodman *et al* 1978 [2]), non-Gaussian imaging (Rees 1982 [3]), optical efficiency enhancement (Ishihara et al 1983 [4]), and retro-reflective screens formation (Daly et al 1990 [5]). More recently, microlens arrays have been widely used in fields such as optical coupling [6, 7], integral imaging [8], diffusers [9], pocket-sized projector [10] and artificial compound eyes etc [11]. Especially, microlens array fabricated at fiber bundle extremity is of great significance for applications, such as vapor sensors [12], localized enhanced Raman scattering (LERS) [13] and particularly remote imaging (remote electrochemiluminescence imaging [14], remote fluorescence imaging [15]).

Many methods of MLA fabrication have been reported [5, 6, 11, 13–20]. They include molding (including thermal reflow technique, sol-gel thermal reflow) [6], self-assembly (including surface wrinkling [16], gel trapping of self-assembly particles [17]), microjet printing [18], laser machining (including irradiation [19], laser melting [5]), and lithography methods [11, 20]. Previous approaches clearly demonstrate the ability and the relevance to generate microlens arrays with uniform profile and controllable size and shape. Nevertheless, certain drawbacks are common for most of them, such as process complexity, high cost, time-consuming and necessity of critical condition.

All the above-mentioned techniques mainly concern the fabrication of MLAs on large planar substrates. Integrating a microlens array at the end of an optical fiber bundle is of great interest for many applications and still constitutes a challenge due to the small-involved surface area of integration. Chovin et al. have developed a chemical etching technique to fabricate a nanostructured array at the extremity of an optical fiber bundle [13–15]. The principle is the utilization of the difference of etching rates between the GeO2-doped core and the fluorine-doped cladding in a selective buffered HF solution. Walt et associates [21–25] developed a protocol to integrate such MLAs at the fiber bundle extremity. Chemical etching is favored on the fiber cores, resulting in array of holes that were subsequently filled by dielectric microspheres acting as microlenses. They aimed to use this structure for different applications including optical sensing [21–25].

In this paper, we present a novel route for the integration of an array of microlenses at the extremity of fiber bundle. It is based on a local photo-induced polymerization process. This process is optimized through control of both exposure dose and geometry of the formulation droplet deposited on the fiber extremity. Our approach presents several advantages over previous reported techniques:

#136713 - $15.00 USD Received 20 Oct 2010; revised 14 Feb 2011; accepted 15 Feb 2011; published 28 Feb 2011

i) Each microlens is fabricated directly by the light emerging from a given core, allowing for an optimal alignment between fiber cores and microlenses;

ii) Lens diameter in controlled within the [1–5] μm range

iii) Lens height can be tuned over a large range;

iv) The full process is very simple and rapid (it lasts a couple of minutes);

v) The process consumes few energy and materials (almost cost-free polymer). In particular exposure power is about hundred nanowatts with an exposure time of several seconds.

2. Experimental

Over the past 10 years, we have been developed an approach of integration of polymer at the extremity of single/multi mode monocored fiber end [26,27]. For the present work, we used the same approach. In particular, we used the same visible-sensitive liquid formulation that polymerizes under green light exposure. The formulation consists of a monomer of pentaerythritol triacrylate (PETIA), a photosensitive dye of eosin Y (2', 4', 5′, 7'-tetrabromofluorescein disodium salt) and a synergist amine of methyldiethanolamine (MDEA). Eosin Y is highly photosensitive from 450 to 550 nm with a maximal peak at 530 nm. Thus, a frequency-doubled Nd/YAG laser (532 nm) has been used to induce the photopolymerization process. A modified route for the integration of an array of polymer lenses on the end facet of an optical fiber bundle with 7×7 arrayed cores is here proposed. The fiber bundle consists of a 7×7 arrayed cores with a core diameter of about 2.6μm and an interdistance of 7.7μm. The refraction indices of the fiber core and the cladding are 1.48 and 1.46, respectively. This approach relies on the control of the volume (thickness) of the photopolymerizable formulation drop deposited at the end of the fiber. The thickness control is monitored by measuring the contact angle of the drop on the fiber end.

The process mainly consists of three steps that are illustrated in Fig. 1:

i) A freshly cleaved fiber (Fig. 1a) is optically characterized in terms of optical transmission and a drop of photopolymerizable formulation is deposited on its extremity. Drop height is reduced to obtain the thickness required. Figure 1b shows the profile of a resulting thin-layered droplet formulation as observed by optical microscopy. The volume of the drop is tailored under control using a micropipette. The green dashed line represents the interface between the solution and the fiber end facet while pink line highlights the profile of the droplet. The contact angle of the droplet on the fiber end was recorded and measured before the exposure. The inset photograph shows a typical droplet profile with a contact angle of 8.5 °.

ii) The formulation is irradiated with a laser beam (λ=532nm, that was coupled into the other fiber extremity) for few seconds to transform the monomers into cross-linked polymer (Fig. 1c);

iii) The fiber end is rinsed with ethanol for several minutes to remove the unpolymerized parts surrounding the polymer tips. The laser power coupled into the other end and emerging at the fiber extremity was measured before the deposition of the droplet. The inset images in Fig. 1a exhibits a typical light transmission property of the multi-cored fiber at wavelength of 532 nm with an incident intensity of 500 nW. In Fig. 1d, the green dashed rectangle highlights the obtained grown microlens array after rinsing. The inset on the bottom-left in Fig. 1d presents a typical optical transmission property after developing while being irradiated by a laser beam with λ=532nm and I = 50nW. The inset on the bottom right in Fig. 1d presents typical obtained polymer microlens array as observed by a scanning electron microscopy (SEM).

#136713 - $15.00 USD Received 20 Oct 2010; revised 14 Feb 2011; accepted 15 Feb 2011; published 28 Feb 2011

3. Analysis and discussions

3.1 Integration of microlens array

The height of the lenses depends on both the thickness of the solution deposited on the fiber end and the exposure dose. Additionally, the concentration variation of the formulation compositions including the monomer, photosensitive dye, synergist and the possible addition of inhibitor greatly influences the results. This point has been discussed in the case of polymer tip integrated on a single mode fiber [26,27] and will be further studied for microlens array in future work. In the present work, we used constant composition, time of exposure (2s) and intensity (I=7μw) for all exposures. On the other hand the influence of the drop geometry was studied (Fig. 2). The contact angle of the droplet was recorded and measured before the exposure. It varied in a large range from several degrees to several tens of degrees. The polymer microlens array heights were determined by SEM cross-sectioned images. Accordingly, we found the correlation between the height of the polymer microlens array and the measured contact angle of the droplet. This provides us a simple way of tuning the height of the MLA.

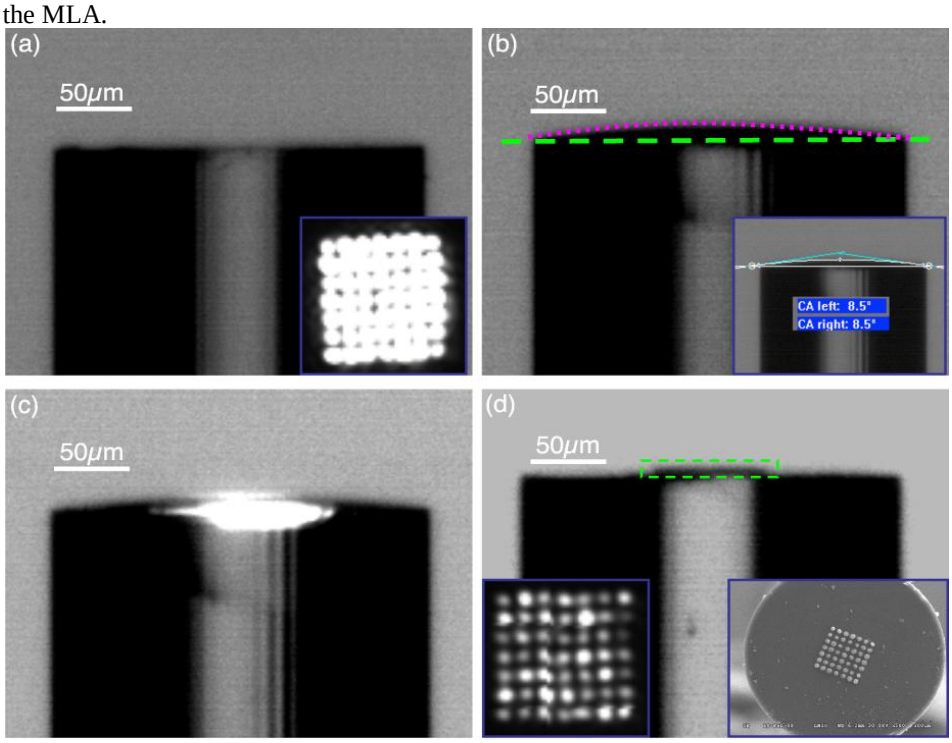

Fig. 1. Fabrication process of a polymer microlens array on a fiber with 7×7 cores by a free radical photopolymerization approach. **a)** Well-cleaved top surface before deposition and a typical light transmission property with an incident intensity of 500nW (inset image); **b)** Droplet profile deposited on the top surface before irradiation and a typical profile with contact angle of 8.5 ° (inset); **c)** Polymerization process under laser irradiation (λ=532nm); **d)** Final structure after unpolymerized formulation removal in ethanol: the inset image on the left showing the optical transmission property while the incident intensity I = 50nW; the inset on the right shows the SEM image of a typical structure of microlens array obtained through this approach.

A contact angle higher than 45° was observed when the fiber was immersed in the liquid formulation and then extracted freely from it. Typically, this angle results in a polymer tip of about 30μm in height. Using a micropipette, the formulation volume and consequently the contact angle can be controlled. We can express the height of the microlens as

#136713 - $15.00 USD Received 20 Oct 2010; revised 14 Feb 2011; accepted 15 Feb 2011; published 28 Feb 2011

$$h = \alpha D \frac{(1-\cos\theta)}{(2\sin\theta)} \quad (1)$$

where α is an empirical value that relies greatly on the surface tension, the properties of the solution and the finite fiber tip dimension. D and θ are the diameter of the fiber end and the measured contact angle, respectively. These two parameters determine the volume and height of the photopolymerization formulation. To illustrate the capability of dimensional control by this route, microlens arrays with different angles measured before exposure are presented in Fig. 2. By reducing the volume under control, thin-layered droplets with different contact angles of 22.9°, 9.3° and 8.5° were obtained (Fig. 2a-c). Their heights, diameters and detailed structures were characterized through SEM cross-sections (Fig. 2d-f), planar arrayed structures (Fig. 2g-i) and more elaborately separate microlens structures (Fig. 2j-l). The average height of microlens array was found to be h=15μm with a contact angle of θ=22.9°. Furthermore, the

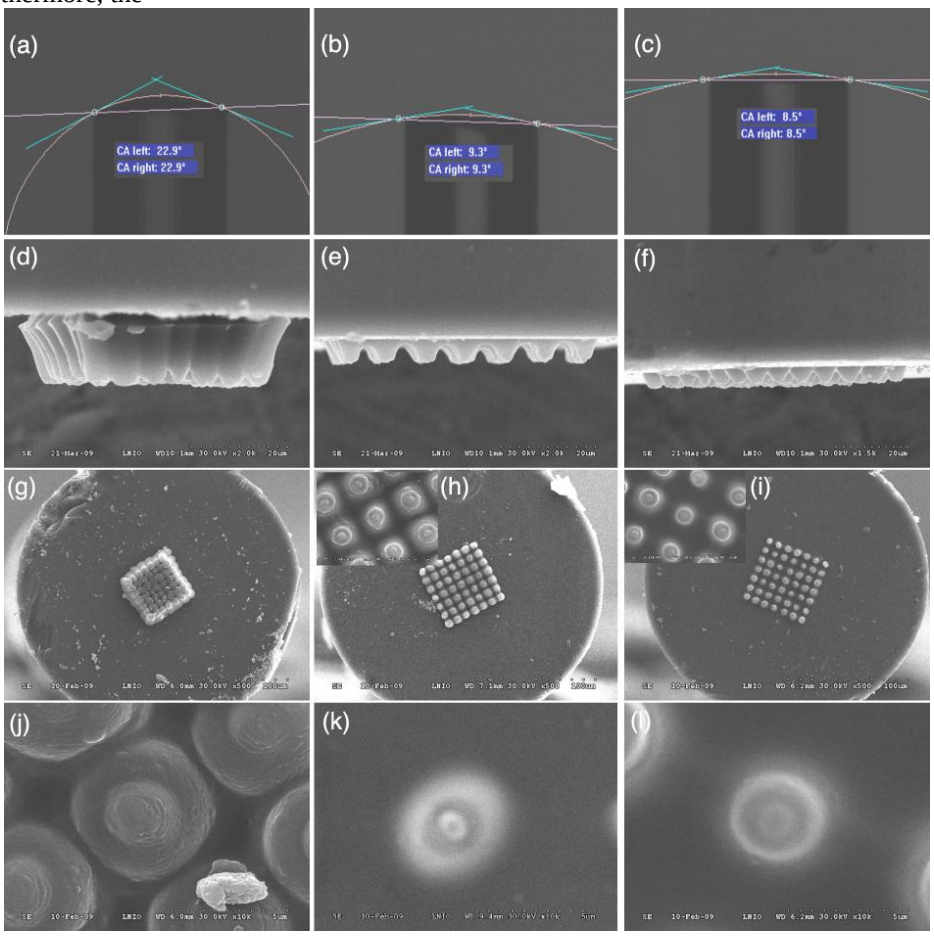

Fig. 2. **a-c)** Measurements of contact angles by optical microscope to control microlens array height h. Using a micropipette, the volume of the droplet is reduced and consequently the contact angle is adjusted to 22.9°, 9.3° and 8.5°, respectively. **d-l)** SEM images show the MLAs fabricated with different contact angles. d-f) Profiles of microlens arrays with different contact angles correspond to a-c, respectively. Microlens array heights in d-f) are about 15μm, 5μm and 4μm, respectively. Interconnection among lenses and rinse trace at these peripheral bottoms in d) can be observed. g-I) exhibit the planar structure of these microlens arrays. A disconnected lens array structure was displayed both in h) and i). The insets are magnification images of lens arrays at their centers. j-l) are local magnification images showing the individual lens structure.

#136713 - $15.00 USD Received 20 Oct 2010; revised 14 Feb 2011; accepted 15 Feb 2011; published 28 Feb 2011

height value of the fabricated polymer lens diminishes with the decrease of the contact angle measured. A rough height of 5μm and 4μm was observed in Fig. 2e and 2f corresponding to measured contact angle value of 9.3° and 8.5°, respectively. As also evidenced in Fig. 2g-h, a large volume of solution coated on the fiber induced a continuous structure while a tiny solution coated may produce an expected isolated microlens array structure. More precisely, an interconnected structure is probably induced for contact angle higher than 15° and a set of well separated microlens is obtained when the contact angle is lower than 10°. A complex structure is observed in Fig. 2j. This structure suggests that the mode inducing the photopolymerization is not the fundamental one (Gaussian mode). A distinct propagation mode was observed in Fig. 2k. This corresponds to a sum of LP11 + LP02 modes. Quasi-hemispherical lens without elongation is shown in Fig. 2l. This result indicates that it is possible to couple a single mode (LP02) in this multicored fiber. As shown by Bachelot et al. [26], the shape of the coupled mode will determine the shape of the polymer microlens. The coefficient αD is deduced from Eq. (1). This value is used to calculate the height of the microlens array from the measured contact angle (θ). For example, for h=15μm and θ=22.9°, the αD value is calculated to be 148. Since the value of α is an empirical value that relies on the surface tension, the properties of the solution and the finite fiber tip dimension. We assume it to be constant. Based on this value of αD, we can calculate the height for different measured contact angles of 8.5°, 9.3°. Then, h is calculated to be equal to 6μm and 5.4μm, respectively. These two calculated values are quite consistent with the heights measured by SEM (~5μm and ~4μm, respectively). Additionally, an interconnected structure tends to form when the contact angle is superior to 15°. Using this calculation, the corresponding height h for this angle is about 9.75μm.

3.2 FDTD simulation for photopolymerization process

A sequence of Finite Difference Time Domain (FDTD) calculations is performed to reveal the evolution of the polymerization process in the initial stage using Rsoft Fullwave. The structure designed for the two dimensional FDTD simulations is illustrated in Fig. 3a. The diameter of each core is about 2.6μm and the distance between them is 7.7μm. The refraction indices of the fiber core and the cladding are 1.48 and 1.46, respectively. Firstly, we consider the structure in air, FDTD simulation results are presented in Fig. 3b. It clearly appears that the light presents a maximum situated at 2μm from the extremity of each core. Moreover, destructive interferences appear in a distance of about 15μm from the fiber end, as denoted by the black dashed boxes. Secondly, we consider the structure in a droplet formulation. The results are shown in Fig. 3c. In this case, we assume the refractive index of the droplet to be 1.48 (without consideration of polymerization) for the simulation. A maximum of intensity is situated at the interface between the fiber and the solution. Thus, the polymerization will be induced at this place. On the other hand, constructive interferences between the different cores are extended from 10μm to 20μm with the maximum at a distance of ~15μm from the fiber end. These interferences will induce a polymerization and then a limitation for the integration of well-separated microlenses. Comparing to the prediction from the Eq. (1), we find that the calculated empirical critical value (9.75μm) is quite consistent with the FDTD simulation results (interferences starting at 10μm).

#136713 - $15.00 USD Received 20 Oct 2010; revised 14 Feb 2011; accepted 15 Feb 2011; published 28 Feb 2011

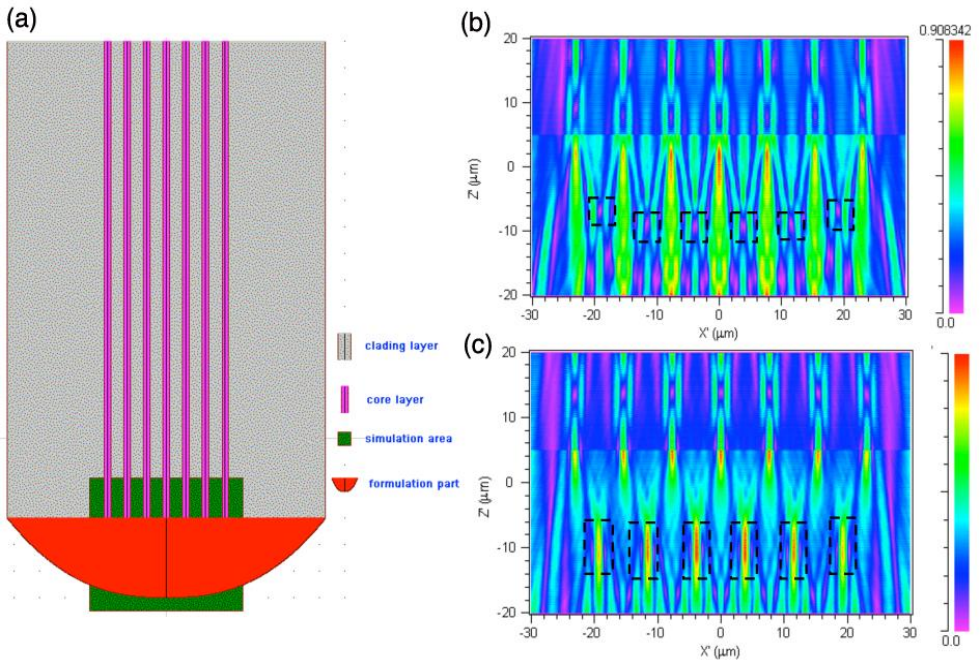

Fig. 3. 2D-FDTD simulations explaining the polymerization process. **a)** Design of the structure; **b)** simulation result without droplet (n_{air}=1); c) simulation result with droplet ($n_{droplet}$=1.48).

3.3 Experimental results of optical transmission

The optical transmission properties for the as-grown microlenses array were performed by using the same frequency-doubled Nd/YAG laser (λ=532 nm) as incident light source. A parallel laser beam was coupled into the fiber from the bare end. It was guided by the multicored fiber to the other end and coupled into the polymer microlens array. Subsequently, the light in transmission was recorded using a CCD, as illustrated in Fig. 4a. The incident intensities for Fig. 4b-d are 50nW, 10nW and 3~4nW, respectively. It clearly appears in Fig. 4c that two different modes have been molded. These two modes are the LP02 and the LP11, as denoted by the red and green broken lines in Fig. 4c, respectively. Moreover, a very low optical signal is measurable (total power of about 3-4nW, i.e. 0.1nW/lens) as shown Fig. 4d. The important point of these measurements is the evidence of the difference of intensities transmitted by the different cores. It comes from the structural difference of the different microlenses induced by the different modes molded. It points out the importance of the experimental details like the coupling of the light in the bundle or the quality of the two extremities of the bundle. In order to reduce these differences, the light must be carefully coupled in the bundle during the integration of the microlenses. Thus, it will be possible to optimize the uniformity of the microlenses.

3.4 FDTD simulation for optical properties of microlens array

In order to obtain a better understanding of the polymer microlens array's optical properties, a simplified polymer microlens structure for two-dimensional FDTD simulations has been considered. The design of the structure for this simulation is illustrated in Fig. 5a. Typically,

#136713 - $15.00 USD Received 20 Oct 2010; revised 14 Feb 2011; accepted 15 Feb 2011; published 28 Feb 2011

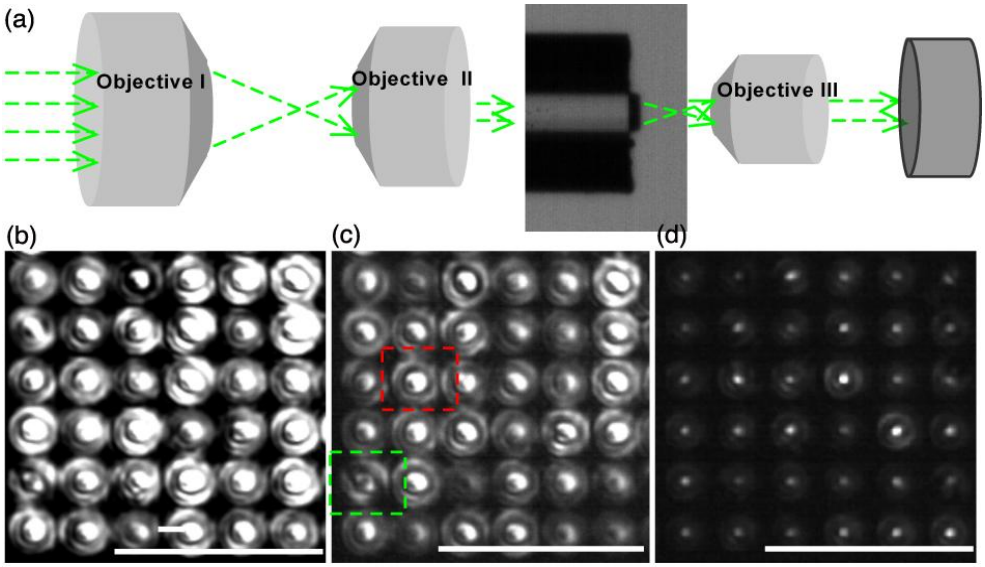

Fig. 4. **a)** Experimental setup used for optical characterization of polymer microlens array. **b-d)** MLA images in transmission recorded with different incident intensities: 50nW, 10nW and 3~4nW were coupled into the multicored fiber, respectively. White-lined scale bars for all images in **b-d)** represent 30μm.

refractive indices of about 1.52 for the polymer lens, 1.48 for the fiber core and 1.46 for the cladding have been considered. The diameter of the fiber core was measured to be 2.6μm and the distance between cores determined to be 7.7μm. The taper structure of the polymer lens was provided by:

$$Z = F(x) = h_0 \left(\frac{w_0 - x}{w_0} \right)^{\alpha}. \tag{2}$$

where h_0 is a constant defined as the height of the polymer tip, w_0 is the half width of the polymer lens on the base, i.e. 1.3μm for our case, and α is the taper shape factor. All these values have been normalized. The conditions used for the simulations are: λ = 532nm, h_0 = 0.5μm and α = 0.5. Simulation results are displayed with coded-color in Fig. 5b. No distinct interference is found during the propagation among fiber and an evident microlens behavior for the polymer component is revealed. Figure 5c and 5d displayed the magnifications for a separate polymer microlens with a coded-color and a contour line mode, respectively. A confined light field with full width at half maximum (FWHM) of the order of 0.4 μm was perceptible. The focal length of the lens is about 2 μm and the field depth is about 1.8 μm.

Based on geometry and optical theory, the focal length (f) and the numerical aperture (NA) can be determined by the following equations [28]:

$$\begin{cases} f = \dfrac{R}{n-1} \\ NA = \sin\left(\arctan \dfrac{D}{2f} \right) \end{cases}. \tag{3}$$

#136713 - $15.00 USD Received 20 Oct 2010; revised 14 Feb 2011; accepted 15 Feb 2011; published 28 Feb 2011

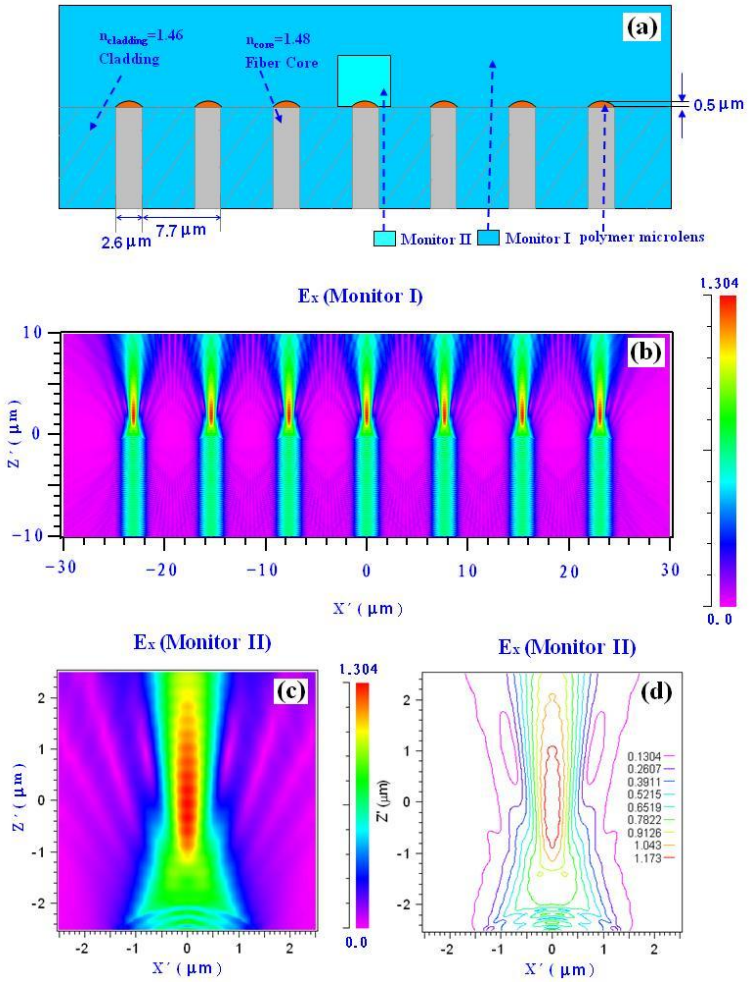

Fig. 5. FDTD simulations (2D) of optical transmission for a single line of polymer microlens array. Simulation conditions are λ=532nm, w_0=1.3µm, h_0=0.5µm and α=0.5. **a)** Scheme showing the structural design for FDTD simulation. **b)** Calculated electric field /E_x/ for seven polymer microlens, **c-d)** Calculated electric field /E_x/ magnifications for an individual polymer microlens with a coded-color and a contour line, respectively.

Where *D*, *n*, *f* and *NA* are the diameter, the refractive index, the focus and the numerical aperture of the polymer lens, respectively. In our case, $D = 2w_0 = 2.6\mu m$, and $n = 1.52$. Taking the calculated focus *f* value of 2µm into consideration, the curvature radius is calculated to be R= 1.04 µm. Consequently, we obtain a numerical aperture *NA* = 0.54 which corresponds to an angle of collection of about 32.6°.

The radius of curvature determines many optical properties of the microlens array. It can be tunable by controlling the polymer lens height and shape. Thus, the control of the volume (or the contact angle) of the droplet of formulation allows us to control the height h_0 of the microlenses. As demonstrated in Fig. 2, h_0 decreases when the contact angle is decreased. The shape factor can be adjusted by employing different exposure dose and varying the compositions of the formulation, i.e. the increase of Eosin Y amount or the addition of inhibitors is favorable to the formation of tiny lens arrays.

#136713 - $15.00 USD Received 20 Oct 2010; revised 14 Feb 2011; accepted 15 Feb 2011; published 28 Feb 2011

4. Conclusion

In summary, we integrated of a microlens array onto a fiber end by a rapid and simple photopolymerization method. We demonstrated the ability to tune the heights of the microlens array by an in situ measurement of the contact angle and the capability to spatially confine the interactional polymerization between microlenses during the polymerization process. It should be noted that microlens matrix without interconnection was achieved provided that the contact angle is small enough (<10°). FDTD simulation supports these results. The direct coupling between the cores and the corresponding microlens enables lots of applications, such as photonic-coupled detectors, parallel optical tweezers or high resolution endoscope. We also believed that the general idea of a polymer microlens array integrated at a fiber bundle extremity is also of great significance for potential applications, such as sensors, remote imaging and localized enhanced Raman spectroscopy.

Acknowledgements

X.H. Zeng thanks the CSC-UT/INSA program for Financial Support. The authors thank the PhLAM Laboratory, IRCICA Institute, Université des Sciences et Technologie de Lille 1 - France, which designed and fabricated the multicore fiber.

#136713 - $15.00 USD Received 20 Oct 2010; revised 14 Feb 2011; accepted 15 Feb 2011; published 28 Feb 2011